NANO LETTERS
Cite This: Nano Lett. XXXX, XXX, XXX−XXX
Letter
pubs.acs.org/NanoLett

Tungsten Disulfide−Gold Nanohole Hybrid Metasurfaces for Nonlinear Metalenses in the Visible Region

Jiawei Chen,[†] Kai Wang,*[,†] Hua Long,[†] Xiaobo Han,[‡] Hongbo Hu,[†] Weiwei Liu,[†] Bing Wang,*[,†] and Peixiang Lu*[,†,‡]

[†]Wuhan National Laboratory for Optoelectronics and School of Physics, Huazhong University of Science and Technology, Wuhan 430074, China

[‡]Laboratory of Optical Information Technology, Wuhan Institute of Technology, Wuhan 430205, China

Supporting Information

ABSTRACT: Recently, nonlinear hybrid metasurface comes into an attractive new concept in the research of nanophotonics and nanotechnology. It is composed of semiconductors with an intrinsically large nonlinear susceptibility and traditional plasmonic metasurfaces, offering opportunities for efficiently generating and manipulating nonlinear optical responses. A high second-harmonic generation (SHG) conversion efficiency has been demonstrated in the mid-infrared region by using multiquantum-well (MQW)-based plasmonic metasurfaces. However, it has yet to be demonstrated in the visible region. Here, we present a new type of nonlinear hybrid metasurfaces for the visible region, which consists of a single layer of tungsten disulfide (WS_2) and a phased gold nanohole array. The results indicate that a large SHG susceptibility of $\sim 10^{-1}$ nm/V at 810 nm is achieved, which is 2−3 orders of magnitude larger than that of typical plasmonic metasurfaces. Nonlinear metalenses with the focal lengths of 30, 50, and 100 μm are demonstrated experimentally, providing a direct evidence for both generating and manipulating SH signals based on the nonlinear hybrid metasurfaces. It shows great potential applications in designing of integrated, ultrathin, compacted, and efficient nonlinear optical devices, such as frequency converters, nonlinear holography, and the generation of nonlinear optical vortex beams.

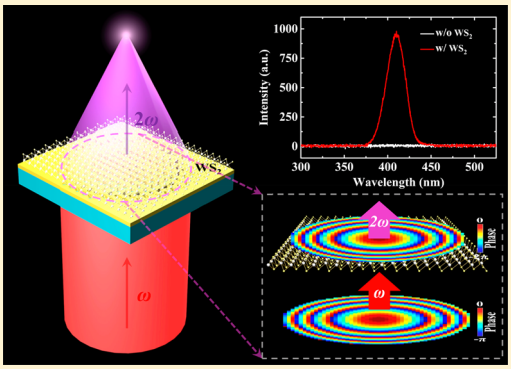

KEYWORDS: *Nonlinear metasurface, hybrid nanostructure, metalens, two-dimensional material, second-harmonic generation*

Optical metasurfaces are a class of artificial nanostructured surfaces with engineered linear optical properties, providing an ideal platform for designing integrated, ultrathin, and compacted planar linear optical devices.[1−9] Recently, this concept has been extended to the nonlinear regime in which nonlinear optical metasurfaces are able to fully control the wavefront of generated nonlinear signals.[10−16] However, this new paradigm faces important challenges because it is required to act as an efficient generator and a subwavelength phase modulator of nonlinear signals simultaneously.

Second-harmonic generation (SHG) is an important second-order nonlinear process that generates photon with twice the fundamental frequency of the pumping laser.[17] Generally, SHG in metal-based (plasmonic) metasurfaces have attracted extensive attentions for applications in the nonlinear regime because plasmonic metasurfaces have an impressive performance in the linear regime with a reliable fabrication technology.[18,19] However, it suffers from a low SHG conversion efficiency due to the inherently weak nonlinear response ($\chi^{(2)} \sim$ pm/V; see Table S1).[18,20] Although it can be boosted by orders of magnitude at resonance condition, the strong absorption losses lead to damage by accumulated heat effect, especially in the visible region. Meanwhile, it might be interfered by the unwanted signals from higher-order nonlinearity, such as white-light supercontinuum (WLC).[21,22] Therefore, only a very low pumping intensity is allowed, showing limitations for practical applications. So far, compared with a large number of works on SHG in metal nanostructures, only a few works have demonstrated the engineered SH signals by plasmonic metasurfaces,[11−13,23] as well as third-harmonic generation (THG)[12,15] and four-wave mixing (FWM).[14]

Alternatively, a scheme of nonlinear hybrid metasurfaces has been proposed by coupling the plasmonic metasurfaces to a highly efficient nonlinear semiconductor. Belkin et al. have demonstrated a remarkably large SHG susceptibility ($\chi^{(2)} \approx 54$ nm/V) in the mid-infrared region (at ~ 8 μm) by a plasmonic metasurface coupled to multiquantum-well (MQW) semiconductor structures.[24,25] Although this hybrid metasurface is suitable for the mid-infrared region, it is unlikely to work in the visible region. The available MQW structures are obviously too thick (~400 nm) for a femtosecond laser excitation at 810 nm

Received: November 29, 2017
Revised: January 23, 2018
Published: January 25, 2018

DOI: 10.1021/acs.nanolett.7b05033
Nano Lett. XXXX, XXX, XXX−XXX

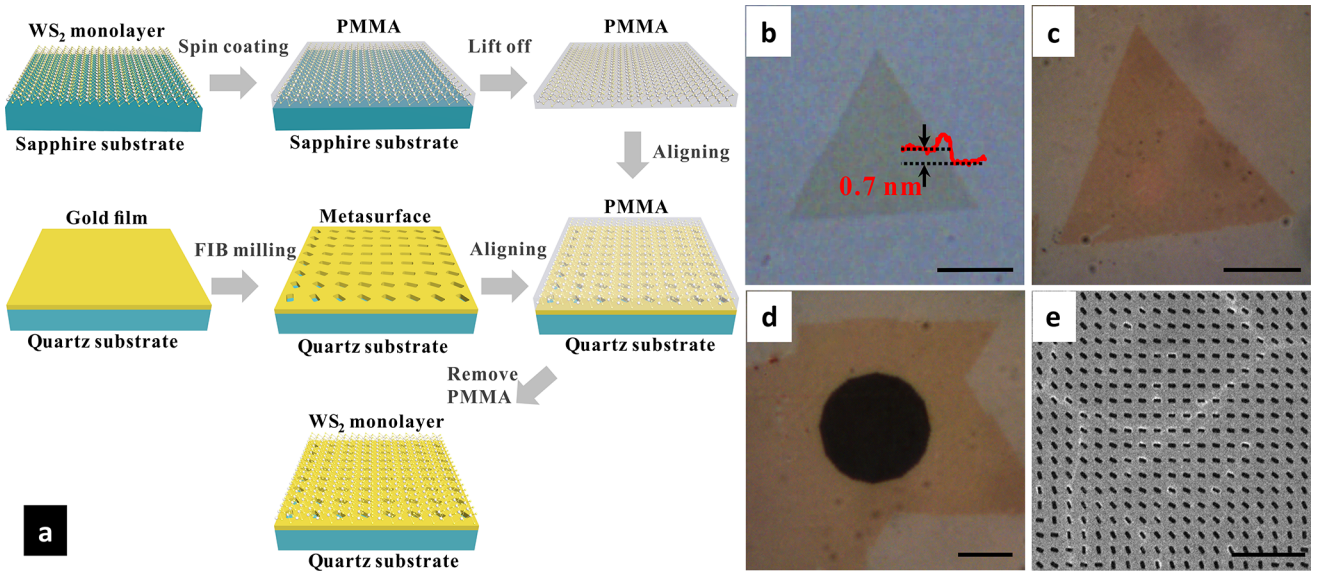

Figure 1. Fabrication of WS_2–gold hybrid metasurfaces. (a) Schematic for transferring WS_2 monolayers onto gold nanohole metasurfaces by the poly(methyl methacrylate) (PMMA)-assisted transfer method. (b,c) The optical images of a WS_2 monolayer before (on sapphire substrate) and after (on gold film) transferring, respectively. The height profile of the WS_2 monolayer was measured by AFM, from which a height of 0.7 nm can be extracted. Scale bars: 20 μm. (d,e) Optical and SEM images of WS_2 on gold nanohole arrays. Scale bars: panel d, 10 μm; panel e, 2 μm.

($\sim\lambda/2$), leading to the problem that the emitted SH signal may be out of phase during its propagation in the MQW structures. More importantly, the intrinsically large nonlinear susceptibility of MQW is $\chi^{(2)}_{zzz}$ that is polarized in the direction normal to the surface. It implies that it is not likely to achieve such a large nonlinear susceptibility with an ultrathin MQW (<40 nm, $\sim\lambda/20$ for ~810 nm). Therefore, it is still quite necessary to demonstrate a new type of nonlinear hybrid metasurface in the visible region. Recently, new types of atomically thin crystals based on layered materials, such as transition metal dichalcogenides (TMD), exhibits excellent physical and chemical properties.[26−28] Specifically, the TMD family of monolayer materials is ultrathin, with a thickness of only one atom and can be easily transferred to the metal nanostructures in a simple approach.[29,30] In addition, characterization of WS_2 and MoS_2 monolayers has also revealed a large intrinsic nonlinear susceptibility, as high as ~nm/V in the visible region.[31−33] Thus, it provides an elegant and promising way to overcome these constraints.

Here, we propose and experimentally demonstrate a new type of nonlinear hybrid metasurfaces in the visible region. It consists of a WS_2 monolayer and a phased gold nanohole array, which is easily prepared by a material transferring method. The gold nanohole array acts as phase plate for the fundamental wave, and the WS_2 monolayer acts as a highly efficient SHG emitter. The results of SHG measurement indicate that a large SHG susceptibility of $\sim 10^{-1}$ nm/V at 810 nm is achieved, which is 2−3 orders of magnitude larger than that of typical plasmonic metasurfaces. The nonlinear metalenses with the focal lengths of 30, 50, and 100 μm are demonstrated experimentally, and the small focal spots of the metalenses are achieved (1−2 μm in diameter). It provides a direct evidence for both efficiently generating and manipulating SH signals based on this nonlinear hybrid metasurfaces, which shows the great potentials to integrated, ultrathin, compacted, and efficient nonlinear optical devices.

Figure 1a shows a brief illustration of the fabrication process of WS_2–gold nanohole hybrid metasurfaces. First, poly(methyl methacrylate) (PMMA) in the anisole solution was drop-coated onto WS_2 flakes supported by a sapphire substrate and baked to remove the solvents. The sample was then immersed in NaOH solution to etch the sapphire substrate and the PMMA–WS_2 film lifted off from the growth substrate. The PMMA–WS_2 film was fished out of the NaOH solution by a glass slide and immersed again in the deionized water, offering a floating PMMA–WS_2 film on the surface of the deionized water. Meanwhile, a gold film was deposited on a quartz substrate and milled with nanopatterns by the focused ion beams (FIB) method. The important step is that the PMMA–WS_2 films were fished out by the fabricated metasurfaces and aligned quickly with the gold nanohole array under an optical microscope. Finally, it was washed in acetone to remove the PMMA coating.

The WS_2 flake grown on the sapphire substrate and the transferred WS_2 flake on gold film are shown in panels b and c in Figure 1, respectively. It can be seen clearly that the triangular WS_2 flakes remain intact after transferring process. The WS_2 flakes used in the experiment is confirmed to be a monolayer with a thickness of 0.7 nm by atomic force microscope (AFM) measurement shown in the inset of Figure 1b. Figure 1d exhibits an optical microscope image of the hybrid metasurface, indicating that the gold nanohole array is fully covered by the WS_2 monolayer. The details of morphology are further characterized by scanning electron microscopy (SEM), shown in Figure 1e. Although the WS_2 monolayer on the gold nanoholes array is in good condition, some tiny cracks are observed in the WS_2 monolayer. It might be induced by the stress relief when the PMMA film was removed. It should be noted that the tiny cracks have a negligible influence on the performance of the hybrid metasurfaces according to the experimental results described below.

A nonlinear metalens was designed for a demonstration of this nonlinear hybrid metasurfaces. Similar to the planar lenses by linear metasurfaces,[34,35] it is crucial that a well-designed phase profile must be imparted to the emitters of nonlinear signals for focusing. In our experiment, it can easily be realized

DOI: 10.1021/acs.nanolett.7b05033
Nano Lett. XXXX, XXX, XXX−XXX

by taking the gold nanoholes array as a phase plate. As shown in Figure 2a, an orientation angle, θ, is defined as the angle between the long-axis of the rectangular gold nanohole and x-axis in the labor frame. When a left (right) circular polarized fundamental beam passes through the rectangular gold nanohole, the transmitted fundamental beam with a right (left) circular polarization is delivered by a geometric phase delay of 2θ while keeping the beam amplitude the same.[35,36] When it further excites the WS_2 monolayer, the emitted SH signal will carry a phase delay of 4θ because SHG is a second-order nonlinear process. Meanwhile, the intensity of the SH signal is uniform and not influenced by the crystal axis of the WS_2 monolayer for its isotropy of the SHG intensity, even under a linearly polarized excitation with different polarization directions.[37] Therefore, the phase of the emitted SH signal can be completely modulated by designing the rectangular gold nanohole with different orientations angle, θ. (More information about the optical property of the gold nanohole and the nonlinear phase control are provided in Figures S1 and S2.) To act like a spherical lens, the phase profile $\varphi(x, y)$ of the nonlinear metalens needs to fit the following equation:

$$\varphi(x, y) = 2\pi(f - \sqrt{x^2 + y^2 + f^2})/\lambda + 2n\pi \quad (1)$$

where λ is the design wavelength, n is an arbitrary integer, x and y are the coordinates of each nanohole, and f is the focal length. Here, we chose λ to be the SH wavelength at 405 nm, and f is equal to 50 μm. The phase profile $2\theta(x, y)$ $(=\varphi(x, y)/2)$ that acts on the WS_2 monolayer is obtained as shown in Figure 2b. Figure 2c exhibits the fabricated rectangular nanoholes array with varied orientations according to the phase profile, and the details of the metasurface are shown in Figure 2d. The total diameter of the fabricated metasurface was 20 μm. Subsequently, a WS_2 monolayer was transferred on the metasurface by using the method described in Figure 1a.

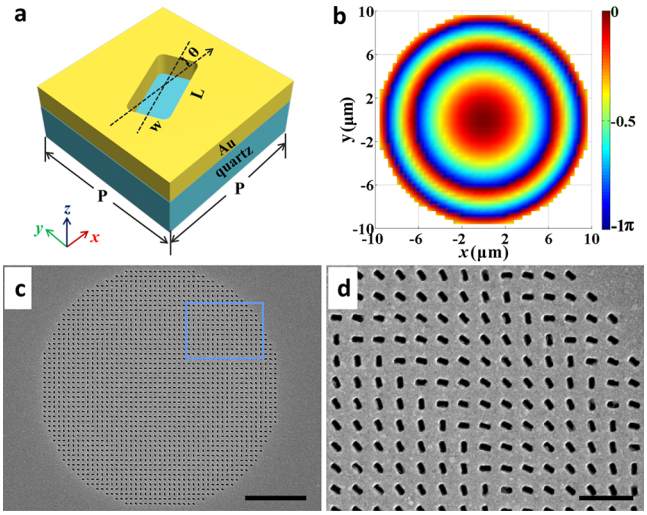

Figure 2. Design and fabrication of the WS_2-gold nanohole hybrid metasurfaces for nonlinear focusing. (a) The geometry of the designed rectangular nanohole unit cell structure in the metasurface, with periodicity $P_x = P_y = 400$ nm. The thickness of gold film is $H = 60$ nm. The nanoslit has length of $L = 185$ nm and width of $W = 80$ nm, and it can rotate in the x-y plane with an orientation angle, θ. All of the sharp corners of the nanoholes are smoothed out by the cylindrical surfaces with a radius of 15 nm. (b) The phase distribution that acts on the WS_2 monolayer for nonlinear focusing with a focal length of 50 μm. (c) The SEM image of the fabricated gold metasurface with rectangular nanoholes of different orientations, θ. The details in the rectangular area are shown in panel d. Scale bars: panel c, 5 μm; panel d, 1 μm.

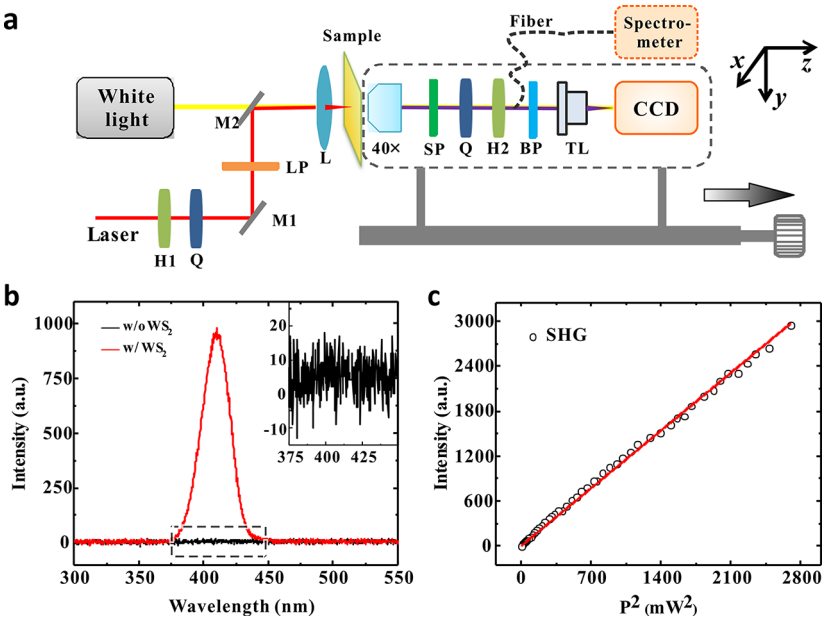

Figure 3. Nonlinear characteristics of hybrid metasurfaces with and without the WS_2 monolayer. (a) The schematic sketch of the experiment setup for SHG and focusing measurements. H1: half-wave plates; H2: Glan-laser polarizer; Q: quarter-wave plate; M1, M2: mirrors; LP: 600 nm long pass filter; SP: 650 nm short pass filter; BP: 400 nm band-pass filter. (b) The nonlinear emission spectra of rectangular nanohole-WS_2 hybrid metasurfaces (w/WS_2) and the bare rectangular nanoholes (w/o WS_2) under the excitation of the circularly polarized fundamental beam. The inset shows the enlarged emission spectrum of the bare rectangular nanoholes. (c) The measured SHG intensity at 405 nm as a function of the square of incident laser power, P^2.

DOI: 10.1021/acs.nanolett.7b05033
Nano Lett. XXXX, XXX, XXX−XXX

Figure 3a illustrates a scheme of a home-built microscope system at room temperature for the SHG measurements. A circular polarized laser was focused by an 8 cm lens, and then it excited the WS_2 monolayer after it passed through the gold nanoholes array. The generated signal was either collected by a spectrometer through a fiber or directly entered into a charge-coupled device (CCD) camera. In Figure 3b, the red curve shows the spectrum of the emitted signal of the hybrid metasurface. It is observed that a sharp peak is located at 405 nm, which is exactly the twice frequency of the pumping laser at 810 nm. Moreover, Figure 3c presents the measured signal intensity as a function of the square of the pumping power, P^2. One can clearly see that the intensity increases linearly with P^2. Thus, it is concluded that the measured signal is ascribed to the SHG response in our experiment.

For comparison, the SH signal of the same bare metasurfaces without a WS_2 monolayer was also measured under the same experimental condition, which is indicated by the black curve in Figure 3b. Obviously, the SHG intensity of the hybrid metasurface is much larger than that of the same bare metasurface, indicating a significant SHG enhancement. For quantitative estimation of the enhancement, we enlarged the spectrum of the bare metasurfaces shown in the inset of Figure 3b. Because it was submerged in background noises, the intensity of SH signal of the bare metasurfaces was estimated to be less than 6 arbitrary units (a.u.) reasonably. A SHG enhancement factor is confirmed to be at least 2 orders of magnitude. Furthermore, we also compared the SHG intensity of the hybrid metasurfaces with that of bare WS_2 monolayer quantitatively, and it indicates a 10 times decrease of SHG conversion efficiency (Figure S4). It has been reported that the WS_2 monolayer possesses a large second-order susceptibility in the level of ~nm/V,[32] and then the second-order susceptibility of our hybrid metasurfaces is at $\sim 10^{-1}$ nm/V. Therefore, the second-order susceptibility of our hybrid metasurfaces is 2−3 orders of magnitude larger than that of typical plasmonic metasurfaces. It is natural that the efficiency of the hybrid film is 10 times lower than that of a bare WS_2 film. Because the bare WS_2 monolayer does not possess the ability of SHG phase control, a gold nanohole array is essential to realize the nonlinear phase control and SHG focusing. Inevitably, the SHG efficiency of the hybrid film is limited by the relatively low transmittance of the laser through the nanoholes (~40% at 810 nm), the dissipation of SHG signal without phase modulation and the absorption of SHG signal by the gold films.

The focusing of the nonlinear metalens based on the hybrid metasurface was determined subsequently. Figure 4a presents the spatial intensity profile of emitted SH signals from the hybrid metasurface located in the center of plane at $z = 0$ μm. An evident converging of SHG along z-axis can be observed, leading to a bright focal spot of SHG. The focal length is measured to be 49 μm, which is consistent with the designing value of 50 μm. Figure 4b shows the intensity distribution of SHG along x-axis at the focal plane ($y = 0$ μm, $z = 49$ μm). The diameter of the SHG focal spot was measured to be ~1.6 μm, while the inset of Figure 4b presents an optical image captured at the focal plane ($z = 49$ μm). Furthermore, the intensity distribution of SHG along z-axis ($x = 0$ μm, $y = 0$ μm) across the focal spot is shown in Figure 4c. It is worth noting that the phase profiles of the hybrid metasurface for the fundamental beam and SH emission are $\varphi(x, y)/2$ and $\varphi(x, y)$, respectively. Thus, the transmitted fundamental beam and SH emission can be separated spatially.

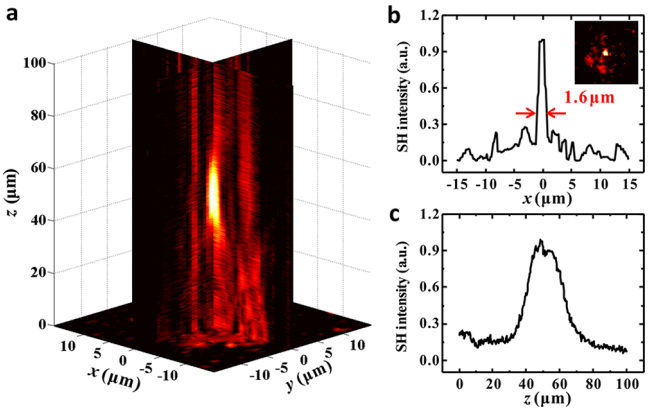

Figure 4. Nonlinear focusing characteristics of the WS_2-gold nanohole hybrid metasurfaces. (a) The experimental results of SHG focusing by using the hybrid metasurfaces. (b,c) The SHG intensity distribution along the x-axis and the z-axis across the center of the focal spot, respectively. The inset of panel b shows the SH beam x−y cross-sections at the focus of 49 μm.

It is convenient to control the focusing behavior by changing the phase profile of nonlinear metalens. We also fabricated nonlinear metalenses with the focal lengths of 30 and 100 μm. According to eq 1, the phase profiles $2\theta(x, y)$ $(=\varphi(x, y)/2)$ that acts on the WS_2 monolayer are acquired for focal lengths of 30 and 100 μm, which is shown in panels a and c of Figure 5, respectively. Figure 5d,f presents the relevant results of the measured nonlinear focusing at $f = 30$ and 100 μm, respectively. Meanwhile, the result for the nonlinear metalens at $f = 50$ μm is also listed in Figure 5b,e for comparison. The diameters of the three focal spots are measured to be in scale of ~1 μm, which is consistent with the result in previous works. (More details are provided in Figure S6.). Moreover, we calculated the 2D linear focusing of the three metalenses with the same phase profile shown in Figure S7. It agrees with the experimental results well, which further supports the nonlinear metalens based on our hybrid metasurface. Therefore, it can be concluded that the hybrid-metasurface based nonlinear metalenses provide an efficient generation of SH signals and effective focusing simultaneously. The arbitrary focal length of the nonlinear metalens can be obtained by a proper design of the metallic nanoholes distributions.

It is worth noting that plasmonics nanohole is suitable for the nonlinear hybrid metasurfaces in our experiment rather than plasmonic nanoatennas. Specifically, it enables "tailoring" of the WS_2 monolayer for controlling SHG because only the fundamental beam that passes through nanoholes can excite the WS_2 monolayer, while the rest is blocked by the unperforated films. This significantly reduces the background noise of SHG. The main drawback of the nanohole is a relatively low transmittance of the fundamental beam, leading to a decrease of the effective SHG conversion efficiency in our hybrid metasurface (~10%). However, it can be significantly improved by changing the phase-control method. Because the metal hole array acts as phase plate for fundamental wave, sophisticated phase-control methods in the linear metasurfaces can be used to control the emitted nonlinear signals in the hybrid nanostructures. It has been reported that the cross-polarization coupling efficiency is fundamentally limited to stay below 25% for the geometric phase,[38] and it can be increased to ~100% by adopting the alternative phase-control method of tailoring the nanostructures size and shape.[39−41] Furthermore, a

DOI: 10.1021/acs.nanolett.7b05033
Nano Lett. XXXX, XXX, XXX−XXX

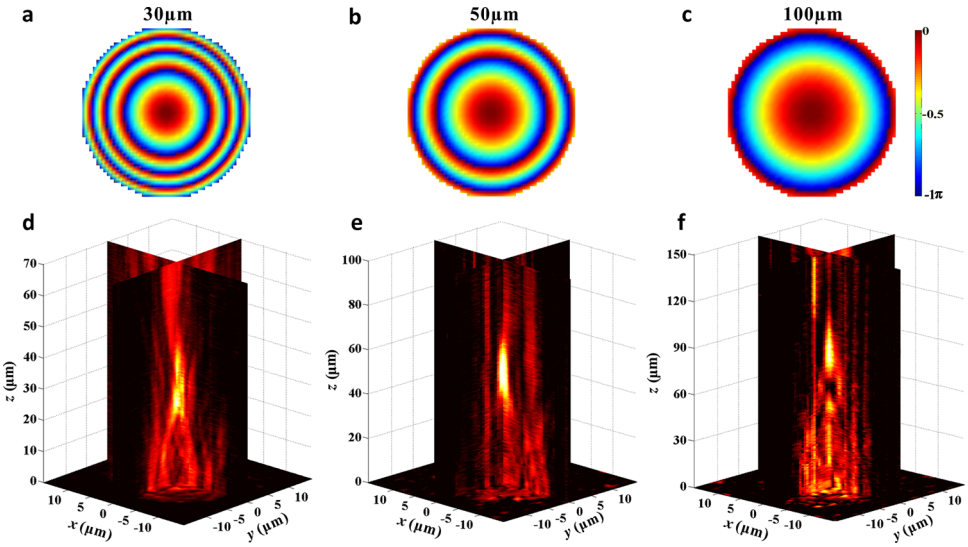

Figure 5. Nonlinear metalenses of focal lengths of 30, 50, and 100 μm based on the WS_2-gold nanohole hybrid metasurfaces. (a–c) The phase distribution that acts on the WS_2 monolayer for nonlinear focusing. (d–f) The metalens experimental measurement of the focal region, respectively.

higher SHG conversion efficiency can be achieved by using low-loss dielectric materials for reducing of the absorption to fundamental beam and SH signals.[42,43] Although only nonlinear focusing is presented in this work, this new type of nonlinear hybrid metasurface is able to realize versatile nonlinear signals manipulation by properly designing the phase profiles of the plasmonic metasurface, such as nonlinear beam direction manipulation, nonlinear vortex beam generation, and nonlinear holography. In addition, a polarization control of the SH emission has also been proved by choosing the hybrid metasurface with constituent gold nanoholes of 3-fold rotational symmetry (Figure S8).

In conclusion, we propose and experimentally demonstrate a new type of nonlinear hybrid metasurfaces for nonlinear transformation optics in the visible region. It consists of a gold-nanohole-based plasmonic metasurfaces coupled to a monolayer of WS_2, which can be easily prepared by a material transferring method. A large SHG susceptibility of $\sim 10^{-1}$ nm/V at 810 nm is achieved, which is 2–3 orders of magnitude larger than that of typical plasmonic metasurfaces. Furthermore, the hybrid metasurfaces effectively suppress any unwanted signals from higher-order nonlinearity (WLC) even under a high pumping intensity, which is proven to be more stable and reliable under an intensive pumping. For the capability of phase modulation, the nonlinear metalenses with the focal lengths of 30, 50, and 100 μm are demonstrated experimentally. It provides a direct evidence for both generating and manipulating SHG signals based on this nonlinear hybrid metasurfaces. From the point of application view, it enables a miniaturized nonlinear optical device with the good performance in a small scale of tens of nanometers. Therefore, it provides a wide range of opportunities for the creation of integrated, ultrathin, ultracompact nonlinear optical devices, such as frequency converters, all-optical switches, and the generation of optical vortex beam as well as nonlinear holography.

Methods. *Sample Fabrication.* The process of sample fabrication included the following steps. (1) For the lift-off of WS_2 monolayer, 1 g of poly(methyl methacrylate) (PMMA, Aldrich, average MW 996 000) was dissolved in anisole to prepare 50 g of solution (2 wt %). A few drops of this solution were drop-coated on the sapphire substrate with WS_2 monolayer flakes until it covered all the substrate. The substrate was then placed at room temperature for 1.5 h for the evaporation of the anisole, followed by a curing step of baking at 120 °C for 0.5 h. Polymer strips about 1 mm wide were scratched by a blade at the edges of the substrate to reduce the lift-off time. The substrate was immersed in 3 mol/L NaOH aqueous solution at 50 °C for more than 4 h to etch the sapphire surface, and the PMMA–WS_2 films would lift off from the growth substrate naturally. The films were fished out with a glass slide and immersed in deionized water for 3 times to remove the residual NaOH solution. (2) The fabrication of gold metasurfaces was accomplished by a focused ion beam milling method. Using an e-beam evaporator, we deposited a 5 nm thick Cr adhesion layer and a 60 nm thick gold layer on a quartz substrate. The different arrangement of nanoholes were milled on the film by means of focused ion beam milling method (FIB, FEI Versa 3D) to generate the metallic metasurfaces. (3) For the combination of the WS_2 monolayers with the gold metasurfaces, with the help of tweezers, the PMMA–WS_2 films were fished out with the fabricated metasurfaces and aligned quickly with the metasurface arrays under the microscope before the water dried. The substrate was then baked at 120 °C for 1 h to improve the combination of WS_2 monolayers with the gold metasurfaces. Finally, the substate was immersed in acetone for 3 times (each time 15 min) to remove the PMMA film.

Experimental Setup and Measurement of SH Signals. A mode-locked Ti-sapphire femtosecond laser centered at 810 nm (Vitara Coherent, 8 fs and 80 MHz) was used for the fundamental beam source. It was filtered spectrally to avoid residual SH from the laser, and its polarization was controlled by a quarter-wave plate. The emission from the sample was collected with an objective lens (Olympus, 40× and 0.65 NA), filtered spectrally, and directly imported to a CCD or through a fiber to a spectrometer (Princeton Instruments Acton 2500i with Pixis CCD camera). The emitted SH signal was extracted by a Glan-laser polarizer with a quarter-wave plate at the SH wavelength.

Measurement of Focusing Effect. A home-built 3D imaging system was used to measure the emitted SH signal profiles from the hybrid metasurfaces under an excitation of a plane-wave

DOI: 10.1021/acs.nanolett.7b05033
Nano Lett. XXXX, XXX, XXX–XXX

laser. The laser was focused by an 8 cm lens to generate the collimated incident fundamental beam. Quarter-wave plates and polarizers were used to generate the circular polarized incident fundamental beam and select SH signals with an opposite circular polarization. To measure the focusing of SHG, we captured the SHG images at the different planes from 0 to 150 μm along the z-axis with a step-size of 0.5 μm. The transmitted SH signal was collected by an objective (40×/0.65) and imaged on a CCD camera.

■ ASSOCIATED CONTENT

Supporting Information

The Supporting Information is available free of charge on the ACS Publications website at DOI: 10.1021/acs.nanolett.7b05033.

Additional details on the optical property of the Au nanoholes, geometric phase-controlled nonlinear signals, SEM images, SHG spectra, nonlinear responses of a bare Au nanohole array and a WS_2−Au nanohole hybrid metasurface, nonlinear metalenses, calculated 2D focusing based on the nonlinear metalenses, polarization-controlled SHG in the hybrid metasurfaces, and a comparison of nonlinear performance based on different materials. (PDF)

■ AUTHOR INFORMATION

Corresponding Authors

*E-mail: kale_wong@hust.edu.cn.
*E-mail: wangbing@hust.edu.cn.
*E-mail: lupeixiang@hust.edu.cn.

ORCID

Kai Wang: 0000-0003-2122-1294

Author Contributions

K.W. and P.X.L. conceived of the experiments; J.W.C and W.W.L. performed the sample fabrication; J.W.C, H.B.H., and X.B.H. performed optical experiments and data analysis; B.W. and H.L. performed theoretical calculations; and K.W. and J.W.C. wrote the manuscript.

Notes

The authors declare no competing financial interest.

■ ACKNOWLEDGMENTS

This work was supported by the 973 Programs under grant no. 2014CB921301 and National Natural Science Foundation of China (nos. 11204097 and 11674117), the Doctoral Fund of Ministry of Education of China under grant no. 20130142110078. Special thanks go to the Center of Nano-Science and Technology of Wuhan University for their support of sample fabrication.

■ REFERENCES

(1) Yu, N.; Capasso, F. *Nat. Mater.* **2014**, *13*, 139−150.
(2) Xu, Y.; Fu, Y.; Chen, H. *Nature Reviews Materials* **2016**, *1*, 16067.
(3) Genevet, P.; Capasso, F.; Aieta, F.; Khorasaninejad, M.; Devlin, R. *Optica* **2017**, *4*, 139−152.
(4) Khorasaninejad, M.; Chen, W. T.; Devlin, R. C.; Oh, J.; Zhu, A. Y.; Capasso, F. *Science* **2016**, *352*, 1190−1194.
(5) Kildishev, A. V.; Boltasseva, A.; Shalaev, V. M. *Science* **2013**, *339*, 1232009.
(6) Ni, X.; Wong, Z. J.; Mrejen, M.; Wang, Y.; Zhang, X. *Science* **2015**, *349*, 1310−1314.
(7) Yu, N.; Genevet, P.; Kats, M. A.; Aieta, F.; Tetienne, J.-P.; Capasso, F.; Gaburro, Z. *Science* **2011**, *334*, 333−337.
(8) Li, X.; Chen, L.; Li, Y.; Zhang, X.; Pu, M.; Zhao, Z.; Ma, X.; Wang, Y.; Hong, M.; Luo, X. *Science Advance* **2016**, *2*, e1601102.
(9) Minovich, A. E.; Miroshnichenko, A. E.; Bykov, A. Y.; Murzina, T. V.; Neshev, D. N.; Kivshar, Y. S. *Laser & Photonics Reviews* **2015**, *9*, 195−213.
(10) Li, G.; Zhang, S.; Zentgraf, T. *Nature Reviews Materials* **2017**, *2*, 17010.
(11) Segal, N.; Keren-Zur, S.; Hendler, N.; Ellenbogen, T. *Nat. Photonics* **2015**, *9*, 180−184.
(12) Li, G.; Chen, S.; Pholchai, N.; Reineke, B.; Wong, P. W.; Pun, E. Y.; Cheah, K. W.; Zentgraf, T.; Zhang, S. *Nat. Mater.* **2015**, *14*, 607−612.
(13) Ye, W.; Zeuner, F.; Li, X.; Reineke, B.; He, S.; Qiu, C. W.; Liu, J.; Wang, Y.; Zhang, S.; Zentgraf, T. *Nat. Commun.* **2016**, *7*, 11930.
(14) Almeida, E.; Shalem, G.; Prior, Y. *Nat. Commun.* **2016**, *7*, 10367.
(15) Almeida, E.; Bitton, O.; Prior, Y. *Nat. Commun.* **2016**, *7*, 12533.
(16) Tymchenko, M.; Gomez-Diaz, J. S.; Lee, J.; Nookala, N.; Belkin, M. A.; Alu, A. *Phys. Rev. Lett.* **2015**, *115*, 207403.
(17) Hu, H.; Wang, K.; Long, H.; Liu, W.; Wang, B.; Lu, P. *Nano Lett.* **2015**, *15*, 3351−3357.
(18) Butet, J.; Brevet, P.-F.; Martin, O. J. *ACS Nano* **2015**, *9*, 10545−10562.
(19) Krasnok, A.; Tymchenko, M.; Alù, A. *Mater. Today* **2017**, DOI: 10.1016/j.mattod.2017.06.007.
(20) Kauranen, M.; Zayats, A. V. *Nat. Photonics* **2012**, *6*, 737−748.
(21) Ko, K. D.; Kumar, A.; Fung, K. H.; Ambekar, R.; Liu, G. L.; Fang, N. X.; Toussaint, K. C. *Nano Lett.* **2011**, *11*, 61−65.
(22) Chen, J.; Wang, K.; Long, H.; Hu, H.; Han, X.; Wang, B.; Lu, P. *Opt. Express* **2017**, *25*, 1296.
(23) Keren-Zur, S.; Avayu, O.; Michaeli, L.; Ellenbogen, T. *ACS Photonics* **2016**, *3*, 117−123.
(24) Lee, J.; Tymchenko, M.; Argyropoulos, C.; Chen, P. Y.; Lu, F.; Demmerle, F.; Boehm, G.; Amann, M. C.; Alu, A.; Belkin, M. A. *Nature* **2014**, *511*, 65−69.
(25) Nookala, N.; Lee, J.; Tymchenko, M.; Sebastian Gomez-Diaz, J.; Demmerle, F.; Boehm, G.; Lai, K.; Shvets, G.; Amann, M.-C.; Alu, A.; Belkin, M. *Optica* **2016**, *3*, 283.
(26) Xia, F.; Wang, H.; Xiao, D.; Dubey, M.; Ramasubramaniam, A. *Nat. Photonics* **2014**, *8*, 899−907.
(27) Basov, D. N.; Fogler, M. M.; Garcia de Abajo, F. J. *Science* **2016**, *354*, aag1992.
(28) Xu, W.; Liu, W.; Schmidt, J. F.; Zhao, W.; Lu, X.; Raab, T.; Diederichs, C.; Gao, W.; Seletskiy, D. V.; Xiong, Q. *Nature* **2017**, *541*, 62−67.
(29) Elías, A. L.; Perea-López, N.; Castro-Beltrán, A.; Berkdemir, A.; Lv, R.; Feng, S.; Long, A. D.; Hayashi, T.; Kim, Y. A.; Endo, M.; et al. *ACS Nano* **2013**, *7*, 5235−5242.
(30) Li, B.; He, Y.; Lei, S.; Najmaei, S.; Gong, Y.; Wang, X.; Zhang, J.; Ma, L.; Yang, Y.; Hong, S.; Hao, J.; Shi, G.; George, A.; Keyshar, K.; Zhang, X.; Dong, P.; Ge, L.; Vajtai, R.; Lou, J.; Jung, Y. J.; Ajayan, P. M. *Nano Lett.* **2015**, *15*, 5089−5097.
(31) Kumar, N.; Najmaei, S.; Cui, Q.; Ceballos, F.; Ajayan, P. M.; Lou, J.; Zhao, H. *Phys. Rev. B: Condens. Matter Mater. Phys.* **2013**, *87*, 161403.
(32) Janisch, C.; Wang, Y.; Ma, D.; Mehta, N.; Elías, A. L.; Perea-López, N.; Terrones, M.; Crespi, V.; Liu, Z. *Sci. Rep.* **2015**, *4*, 5530.
(33) Merano, M. *Opt. Lett.* **2016**, *41*, 187−190.
(34) Hu, J.; Liu, C. H.; Ren, X.; Lauhon, L. J.; Odom, T. W. *ACS Nano* **2016**, *10*, 10275−10282.
(35) Chen, X.; Huang, L.; Muhlenbernd, H.; Li, G.; Bai, B.; Tan, Q.; Jin, G.; Qiu, C. W.; Zhang, S.; Zentgraf, T. *Nat. Commun.* **2012**, *3*, 1198.
(36) Bomzon, Z. e.; Kleiner, V.; Hasman, E. *Opt. Lett.* **2001**, *26*, 1424−1426.
(37) Liang, J.; Zhang, J.; Li, Z.; Hong, H.; Wang, J.; Zhang, Z.; Zhou, X.; Qiao, R.; Xu, J.; Gao, P.; Liu, Z.; Liu, Z.; Sun, Z.; Meng, S.; Liu, K.; Yu, D. *Nano Lett.* **2017**, *17*, 7539−7543.

DOI: 10.1021/acs.nanolett.7b05033
Nano Lett. XXXX, XXX, XXX−XXX

(38) Ding, X.; Monticone, F.; Zhang, K.; Zhang, L.; Gao, D.; Burokur, S. N.; de Lustrac, A.; Wu, Q.; Qiu, C. W.; Alu, A. *Adv. Mater.* **2015**, *27*, 1195−1200.
(39) Arbabi, A.; Arbabi, E.; Horie, Y.; Kamali, S. M.; Faraon, A. *Nat. Photonics* **2017**, *11*, 415−420.
(40) Pors, A.; Bozhevolnyi, S. I. *Opt. Express* **2013**, *21*, 27438.
(41) Qin, F.; Ding, L.; Zhang, L.; Monticone, F.; Chum, C. C.; Deng, J.; Mei, S.; Li, Y.; Teng, J.; Hong, M.; et al. *Science advances* **2016**, *2*, e1501168.
(42) Kuznetsov, A. I.; Miroshnichenko, A. E.; Brongersma, M. L.; Kivshar, Y. S.; Luk'yanchuk, B. *Science* **2016**, *354*, aag2472.
(43) Wang, L.; Kruk, S.; Tang, H.; Li, T.; Kravchenko, I.; Neshev, D. N.; Kivshar, Y. S. *Optica* **2016**, *3*, 1504.

DOI: 10.1021/acs.nanolett.7b05033
Nano Lett. XXXX, XXX, XXX−XXX